Electronic Supplementary Information: Light-Induced C–H Activation on Single-Atom Doped Plasmonic Silver Nanoparticles

R. Sundheep[1] and Hyun Woo Kim[1,2,*]

[1] *Department of Chemistry, Gwangju Institute of Science and Technology, Gwangju, 61005, Korea*

[2] *Center for Quantum Technology, Korea Institute of Science and Technology, Seoul, 02792, Korea*

CONTENTS

S1. Computational Methods 2

S2. Machine Learning 3

S2.1. Alloy atom elemental features 3

S2.2. DFT-based Descriptors 4

S2.3. SISSO 5

S3. TDDFT 7

S4. Adsorption Pathways 8

S5. Input Files 9

S5.1. VASP 9

S5.2. OCTOPUS 9

References 10

S1. COMPUTATIONAL METHODS

Geometry optimizations were performed using the Vienna Ab initio simulation package (VASP).[1] The electron-ion interaction was described using the projector-augmented wave (PAW) potentials,[2,3] and the exchange correlation was modeled using the local density approximation (LDA).[4,5] Plane waves with an energy cutoff of 500.0 eV were used for expanding the Kohn-Sham (KS) orbitals and each structure was relaxed in a cubic box with side length of 18.0 Å. The force and energy convergence thresholds used for the relaxations were 0.02 eV/Å and 0.01 meV/atom respectively. To begin the relaxation, CH_4 molecule was placed at a distance of 3.00 Å from the top most silver atom of the silver nanoparticle. Note that the distance here refers to the distance between the apex Ag atom in the Ag nanoparticle and the center of the H atom in methane closest to the Ag nanoparticle. The alloyed nanoparticles were generated by replacing the silver atom (tip atom) closest to the hydrogen atom of the CH_4 molecule. Geometric optimizations were carried out for the created nanoparticles and the integrated crystal Hamilton population (ICOHP) the Bader charges and the adsorption energy were calculated for the optimized geometries to quantify the interaction between dopant atom and the H atom of CH_4. The geometry optimizations were carried out by aligning the vector connecting the tip Ag atom and the nearest H atom in CH_4 along the molecular y-axis.

The ground state electronic structure calculations, employing DFT[6] and excited state properties employing RT-TDDFT,[7] were carried out using real-space code OCTOPUS.[8–10] The simulation zone was defined by assigning a sphere around each atom with a radius of 8 Å and a spacing of 0.19 Å between grid points. As the system is treated as an isolated molecule in this setup dipole corrections were not included in the calculations. The interaction between the valence electrons and atomic core were represented using PSF/Troullier-Martins pseudopotentials.[11] Ground state calculations showed that the total spin of the molecular system is zero. Hence, all calculations are carried out at the LDA exchange correlation functional level of theory without including spin polarisation. However, since spin polarisation could be important in some cases, we additionally performed test calculations and confirmed that including spin polarisation does not affect the computational results. A time step of 0.002 $\hbar/eV \approx 0.0013\ fs$ was used for all the RT-TDDFT simulations. The parameters were chosen in a way that balanced computational efficiency and accuracy. The electron-nuclear dynamics was treated using the Ehrenfest dynamics.[12] An approximated enforced time-reversal symmetry algorithm[13] implemented in the octopus package was used for simulating excited state dynamics. Laser pulse with a Gaussian wave packet, having a frequency of 3.40 eV, was applied to the system, $E(\omega, t) = E_{max} exp[-\frac{(t-t_0)^2}{2\tau^2}] cos(\omega(t-t_0))$, where

$\tau = 4\ fs$ and the laser field reached its maximum amplitude E_{max} at the time $t_0 = 15.8\ fs$. The laser field is applied along the molecular y-axis and along a perpendicular direction to study the effect of laser field direction on the bond length variation Δr_{max} of the adsorbed molecule in the nanoparticle system. Optical absorption spectra of the antenna reactors were obtained by propagating the electronic density for a duration of $15fs$ employing the Yabana-Bertsch formalism of RT-TDDFT.[14]

S2. MACHINE LEARNING

S2.1. Alloy atom elemental features

For the creation of a basic machine learning model, 21 atoms were used to replace the Ag atom closest to the CH_4 molecule. The atoms used in this study are Pt, Ir, Rh, Mo, Au, Ag, Sc, Ca, Ni, Pd, Ta, Hg, V, P, Cr, Cu, Cd, Zn, Na, Mg and Ga. The elemental features of the alloy atoms used in the study are tabulated below. The elemental features of the alloy atom was extracted using Pymatgen python package.[15]

TABLE S1. The elemental features used in SISSO models.

S.No.	Features
1	Z
2	group
3	row
4	Electronegativity (X)
5	Ionization Energy
6	Electron affinity
7	Density of solid
8	atomic mass
9	atomicradius
10	molar volume
11	boiling point
12	melting point
13	average ionic radius
14	no of d electrons

S2.2. DFT-based Descriptors

The DFT-based descriptors used in this work included the distance between the tip atom and H atom of the CH_4 molecule, ICOHP, Bader charge and the adsorption energy of the relaxed alloyed antenna structures.

After relaxing the alloy antenna nanostructures using VASP, the distance between the alloy atom and the H atom was calculated. The lowest and highest distances of the alloy nanoparticles observed after geometry relaxation are $1.91\mathring{A}$ (Rh dopant) and $3.34\mathring{A}$ (Ni dopant), respectively. Interestingly, however, the shortest distance between the Rh dopant and the H atom was not directly correlated with the extent of C–H bond activation after laser illumination. In the absence of laser illumination, the short Rh–CH_4 distance yields a Δr_{max} of 0.0318 Å, compared with 0.013 Å for Ga and 0.025 Å for Ag. Under laser illumination, the corresponding Δr_{max} values increase to 0.0932 Å, 0.318 Å, and 0.193 Å for Rh, Ag, and Ga, respectively as shown in Table S2. These observations motivated us to expand our set of descriptors to include ICOHP values and Bader charges.

TABLE S2. Distance versus ICOHP, Bader Charge and Δr_{max} for representative elements.

Element	Distance Å	ICOHP	Bader Charge	Δr_{max} No Laser	Δr_{max} with Laser
Rh	1.9072	-0.2732	-0.1581	0.0318	0.0932
Ag	2.1977	-0.1664	-0.0014	0.0255	0.1930
Ga	2.8899	0.0027	0.3117	0.0125	0.3179
Ni	3.3447	-0.0369	-0.0268	0.0189	0.2341

The ICOHP values for the alloyed antenna nanostructures were calculated using the LOBSTER code.[16] A default local basis set provided by Koga et al[17] were used for the projections. The reliability of the calculations was ensured by monitoring the charge spilling percentage. The absolute total spilling during the calculations was below 5%.

The Bader decomposition of electron density[18] after relaxation calculations were carried out using the code provided by Henkelmen et.al[19]

The adsorption energy of the alloy antenna structures was calculated using the formula

$$\text{ads energy} = E_{CH_4+NP} - E_{NP} - E_{CH_4} \tag{S1}$$

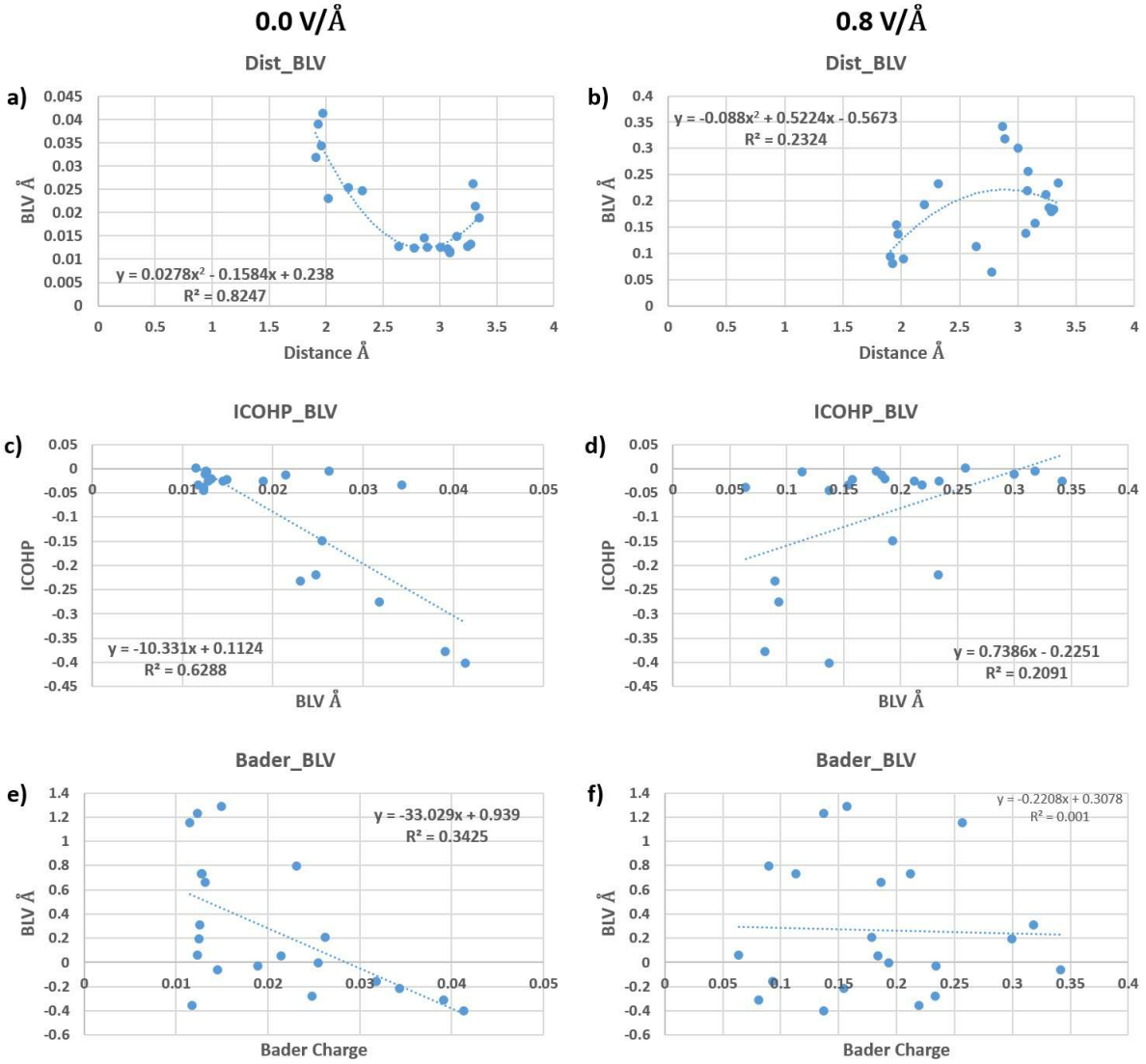

FIG. S1. Trend in the variation of DFT features with alloy atoms a) & b) Distance between the tip alloy atom and H atom, c) & d) ICOHP values and e) & f) Bader charges. Here "Per"/"Par" refers to the application of laser perpendicular/parallel to the axis containing tip alloy atom and H atom of CH_4 respectively

S2.3. SISSO

In order to check the feasibility of developing a basic machine learning model with elemental and DFT features, we used the TorchSISSO package[20]. For model training, the number of feature expansions and the number of terms in the final equation was kept at 3. The equation given by SISSO in the absence of laser radiation is given below.

$$0.0354884325 \times ((\text{no of d electrons/Distance})/(\text{Distance} \times \text{molar volume}))$$
$$+0.0237013709 \times ((\text{no of d electrons/Z})/(\text{no of d electrons-molar volume}))$$
$$+0.0000094028 \times ((\text{Distance - molar volume}) \times (\text{Distance} \times \text{no of d electrons})) + 0.01270374952931343 \quad \text{(S2)}$$

The RMSE value and the R^2 score for the case without laser irradiation were 0.00171 and 0.966, respectively. In the presence of laser irradiation, the equation connecting the input features and the bond length variation was found to be

$$-0.0535917440 \times (\text{melting point-(ads energy} \times \text{X}))$$
$$+0.0139269889((\text{ads energy+melting point})/(\text{Distance/X})) \quad \text{(S3)}$$
$$+0.0026960491((\text{ads energy/melting point})/(\text{ads energy+Distance})) + 0.2187157888379296$$

The RMSE value and the R^2 score for the case with laser irradiation were 0.02616 and 0.881, respectively. The difference in final features determining the bond length variation with and without laser irradiation indicates that constructing a basic machine learning model with atomic features and ground state DFT calculations was not straight forward.

S3. TDDFT

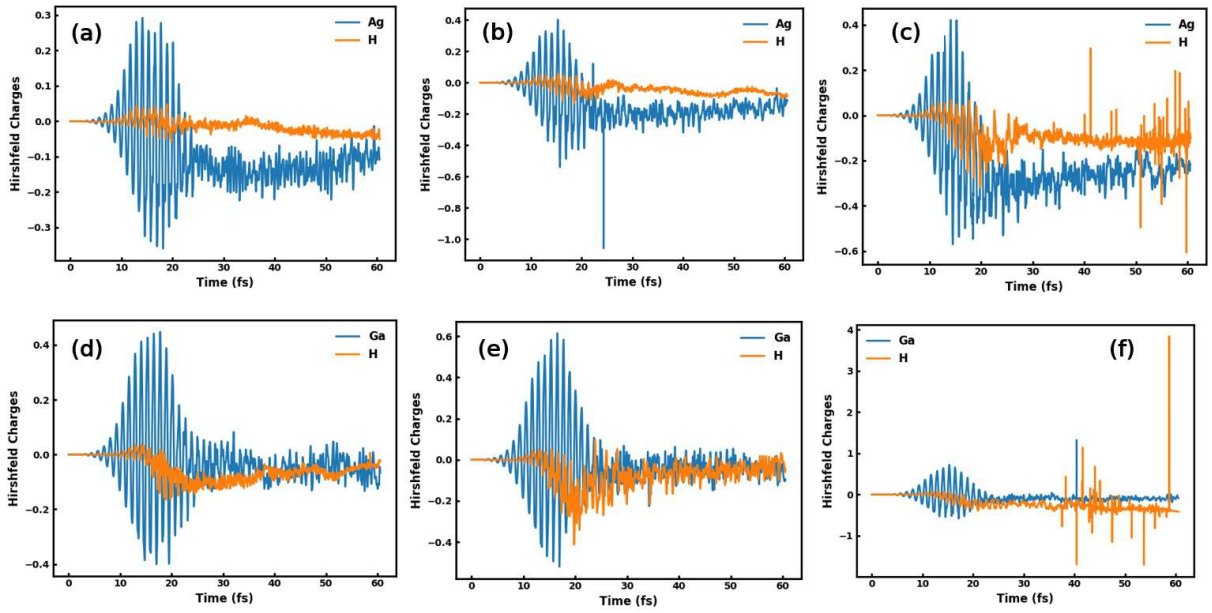

FIG. S2. Variation in the Hirshfeld charges for a laser intensity of (a) 0.8 eV/Å, (b) 1.2 eV/Å, (c) 1.6 eV/Å for the $Ag_{20}-CH_4$ alloy reactor system and (d) 0.8 eV/Å, (e) 1.2 eV/Å, (f) 1.6 eV/Å for the $GaAg_{20}-CH_4$ alloy reactor system. The H atom closest to the alloy catalyst was used for charge analysis.

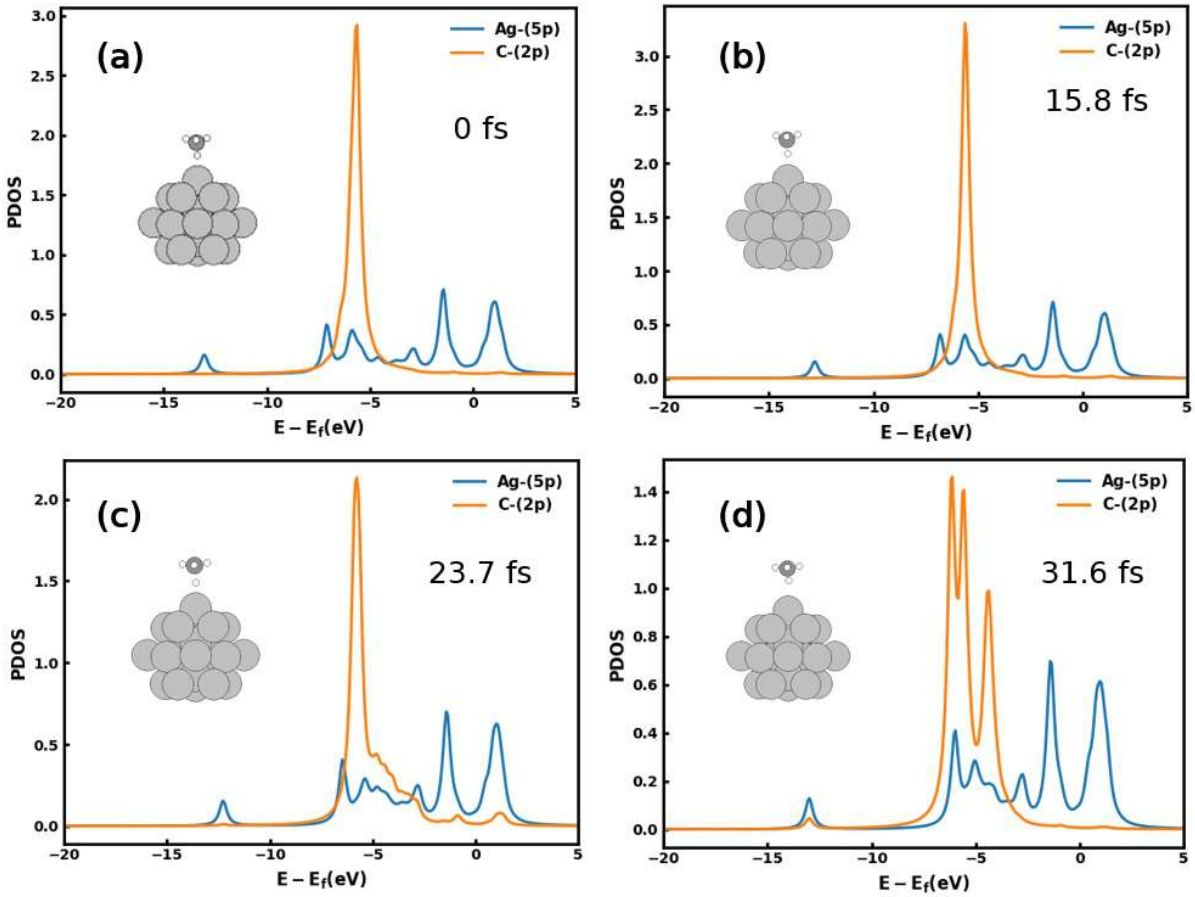

FIG. S3. PDOS of Ag−CH_4 at (a) 0 fs, (b) 15.8 fs, (c) 23 .7 fs and (d) 31.6 fs of the time dependent DFT simulation with a laser intensity of 1.2 V/Å. The inset images show the structure of Ag−CH_4 at the corresponding simulation time. Compared to GaAg−CH_4, it is observed that there is no p orbital interaction between Ag and CH_4 and no bond activation

S4. ADSORPTION PATHWAYS

In our simulations of the Ga-doped system, C-H bond activation in CH_4 leads to H adsorption on the surface while CH_3 remains in the gas phase. Since both fragments do not adsorb, this is not a classical dissociative adsorption. Consequently, the Eley-Rideal (E-R) and Langmuir-Hinshelwood (L-H) mechanisms are not directly applicable at this stage. However, if CH_3 later adsorbs on the surface, forming $CH_3\cdot$ and $H\cdot$, the L-H mechanism could become relevant.

S5. INPUT FILES

S5.1. VASP

The parameters used in the INCAR file for ground state relaxation of Ag−CH_4 and doped Ag−CH_4 molecular system is given below

ENCUT = 500.000000

SIGMA = 0.200000

EDIFF = 1.00e-05

EDIFFG = -2.00e-02

ALGO = Fast

PREC = accurate

IBRION = 1

ISIF = 2

ISMEAR = 1

NSW = 200

LREAL = Auto

S5.2. OCTOPUS

The parameters used in the "inp" file for RT-TDDFT simulations using octopus is given below

CalculationMode = td

UnitsOutput = eV_Angstrom

%Species

'Ag' | species_pseudo | set | standard

'Ag' | species_pseudo | set | standard

%

XYZcoordinates = 'AgAgch4_relaxed.xyz'

Radius = 8.0*angstrom

Spacing = 0.19*angstrom

ExperimentalFeatures = yes

TDPropagator = aetrs

TDMaxSteps = 46000

TDTimeStep = 0.002/eV

MoveIons = yes

ConvRelDens = 1.0e-10

amplitude = 1.2*eV/angstrom

omega = 3.40*eV

tau0 = 4.0*fs

t0 = 15.8*fs

%TDExternalFields

electric_field | 0 | 1 | 0 | omega | "envelope_cos"

%

%TDFunctions

"envelope_cos" | tdf_gaussian | amplitude | tau0 | t0

%

%TDOutput

laser

multipoles

partial_charges

%

MaximumIter = 1000

---

*

[1] G. Kresse and J. Furthmüller, Comput. Mater. Sci. **6**, 15 (1996).

[2] G. Kresse and D. Joubert, Phys. Rev. B **59**, 1758 (1999).

[3] P. E. Blöchl, Phys. Rev. B **50**, 17953 (1994).

[4] D. M. Ceperley and B. J. Alder, Phys. Rev. Lett. **45**, 566 (1980).

[5] J. P. Perdew and A. Zunger, Phys. Rev. B **23**, 5048 (1981).

[6] W. Kohn and L. J. Sham, Phys. Rev. **140**, A1133 (1965).

[7] E. Runge and E. K. U. Gross, Phys. Rev. Lett. **52**, 997 (1984).

[8] N. Tancogne-Dejean, M. J. T. Oliveira, X. Andrade, H. Appel, C. H. Borca, G. Le Breton, F. Buchholz, A. Castro, S. Corni, A. A. Correa, U. De Giovannini, A. Delgado, F. G. Eich, J. Flick, G. Gil, A. Gomez, N. Helbig, H. Hübener, R. Jestädt, J. Jornet-Somoza, A. H. Larsen, I. V. Lebedeva, M. Lüders, M. A. L. Marques, S. T. Ohlmann, S. Pipolo, M. Rampp, C. A. Rozzi, D. A. Strubbe, S. A. Sato, C. Schäfer, I. Theophilou, A. Welden, and A. Rubio, J. Chem. Phys. **152**, 124119 (2020), https://pubs.aip.org/aip/jcp/article-pdf/doi/10.1063/1.5142502/16712083/124119_1_online.pdf.

[9] A. Castro, H. Appel, M. Oliveira, C. A. Rozzi, X. Andrade, F. Lorenzen, M. A. L. Marques, E. K. U. Gross, and A. Rubio, Phys. Status Solidi B **243**, 2465 (2006), https://onlinelibrary.wiley.com/doi/pdf/10.1002/pssb.200642067.

[10] M. A. Marques, A. Castro, G. F. Bertsch, and A. Rubio, Comput. Phys. Commun **151**, 60 (2003).

[11] N. Troullier and J. L. Martins, Phys. Rev. B **43**, 1993 (1991).

[12] A. D. McLachlan, Mol. Phys. **8**, 39 (1964).

[13] A. Castro, M. A. L. Marques, and A. Rubio, J. Chem. Phys. **121**, 3425 (2004), https://pubs.aip.org/aip/jcp/article-pdf/121/8/3425/19313892/3425_1_online.pdf.

[14] K. Yabana and G. F. Bertsch, Phys. Rev. B **54**, 4484 (1996).

[15] S. P. Ong, W. D. Richards, A. Jain, G. Hautier, M. Kocher, S. Cholia, D. Gunter, V. L. Chevrier, K. A. Persson, and G. Ceder, Comput. Mater. Sci **68**, 314 (2013).

[16] S. Maintz, V. L. Deringer, A. L. Tchougréeff, and R. Dronskowski, J. Comput. Chem. **37**, 1030 (2016), https://onlinelibrary.wiley.com/doi/pdf/10.1002/jcc.24300.

[17] T. Koga and A. J. Thakkar, J. Phys. B At. Mol. Opt. Phys. **29**, 2973 (1996).

[18] R. F. W. Bader, Chem. Rev **91**, 893 (1991).

[19] G. Henkelman, A. Arnaldsson, and H. Jónsson, Comput. Mater. Sci **36**, 354 (2006).

[20] M. Muthyala, F. Sorourifar, and J. A. Paulson, Digit. Chem. Eng **13**, 100198 (2024).